online data

Proximal mutations at the type 1 copper site of CotA laccase: spectroscopic, redox, kinetic and structural characterization of I494A and L386A mutants

Paulo DURÃO*, Zhenjia CHEN*, Catarina S. SILVA*, Cláudio M. SOARES*, Manuela M. PEREIRA*, Smilja TODOROVIC*, Peter HILDEBRANDT†, Isabel BENTO*, Peter F. LINDLEY* and Lígia O. MARTINS*[1]

*Instituto de Tecnologia Química e Biológica, Universidade Nova de Lisboa, Av. da República, 2781-901 Oeiras, Portugal, and †Technische Universität Berlin, Institut für Chemie, Sekr. PC 14, Straße des 17. Juni 135, D-10623 Berlin, Germany.

In the present study the CotA laccase from *Bacillus subtilis* has been mutated at two hydrophobic residues in the vicinity of the type 1 copper site. The mutation of Leu^{386} to an alanine residue appears to cause only very subtle alterations in the properties of the enzyme indicating minimal changes in the structure of the copper centres. However, the replacement of Ile^{494} by an alanine residue leads to significant changes in the enzyme. Thus the major visible absorption band is upshifted by 16 nm to 625 nm and exhibits an increased intensity, whereas the intensity of the shoulder at approx. 330 nm is decreased by a factor of two. Simulation of the EPR spectrum of the I494A mutant reveals differences in the type 1 as well as in the type 2 copper centre reflecting modifications of the geometry of these centres. The intensity weighted frequencies $<\nu_{Cu-S}>$, calculated from resonance Raman spectra are 410 cm^{-1} for the wild-type enzyme and 396 cm^{-1} for the I494A mutant, indicating an increase of the Cu–S bond length in the type 1 copper site of the mutant. Overall the data clearly indicate that the Ile^{494} mutation causes a major alteration of the structure near the type 1 copper site and this has been confirmed by X-ray crystallography. The crystal structure shows the presence of a fifth ligand, a solvent molecule, at the type 1 copper site leading to an approximate trigonal bipyramidal geometry. The redox potential of the L386A and I494A mutants are shifted downwards by approx. 60 and 100 mV respectively. These changes correlate well with decreased catalytic efficiency of both mutants compared with the wild-type.

Key words: CotA laccase, laccase, multi-copper oxidase, T1 copper, site-directed mutagenesis.

INTRODUCTION

Laccases are the simplest members of the MCO (multi-copper oxidase) family of enzymes that includes ascorbate oxidase (L-ascorbate oxygen oxidoreductase, EC 1.10.3.3) and ceruloplasmin [Fe(II) oxygen oxidoreductase, EC 1.16.3.1]. MCOs are characterized by having four copper(II) ions that are classified into three distinct types of copper sites, namely type 1 (T1), type 2 (T2) and type 3 (T3) [1–4]. The classical T1 copper site comprises two histidine residues and a cysteine residue arranged in a distorted trigonal geometry around the copper ion with bonding distances approx. 2.0 Å (1 Å = 0.1 nm); a weaker fourth methionine ligand completes the tetrahedral geometry with a Cu–S distance of approx. 3.2 Å. The copper–cysteine linkage is characterized by an intense $S(\pi) \rightarrow Cu(d_{x^2-y^2})$ CT (charge transfer) absorption band at approx. 600 nm, the origin of an intense blue colour of these enzymes, and a narrow parallel hyperfine splitting [$A_{\parallel} = (43–90) \times 10^{-4}$ cm^{-1}] in the EPR spectrum. Upon excitation into the CT band, the RR (resonance Raman) spectra of blue copper proteins typically display several bands between 350 and 430 cm^{-1} involving the Cu–S(cysteine) stretching co-ordinates. The intensity weighted frequency average of these modes allows estimation of the Cu–S bond length and thus provides insight into the T1 site geometry [5]. The function of the T1 copper site is to shuttle electrons from substrates (via one of the histidine ligands oriented towards the molecular surface) to the trinuclear copper centre where molecular oxygen is reduced to two molecules of water during the complete four-electron catalytic cycle. The trinuclear centre contains a T2 copper co-ordinated by two histidine residues and one water molecule, lacks strong absorption bands and exhibits a large parallel hyperfine splitting in the EPR spectrum [$A_{\parallel} = (150–201) \times 10^{-4}$ cm^{-1}]. The T2 copper site is in close proximity to two T3 copper ions, which are each co-ordinated by three histidine residues and typically coupled, for example, through a hydroxide bridge. The T3 or coupled binuclear copper site is characterized by an intense absorption band at 330 nm originating from the bridging ligand and by the absence of an EPR signal due to the antiferromagnetical coupling of the copper ions.

The catalytic rate-limiting step in laccases is considered to be the oxidation of the substrate at the T1 copper site, which switches between the +1 and +2 redox states [1]. The reduction potential of the copper(II)/copper(I) couple is thus a crucial physico-chemical parameter for the enzyme function. Understanding molecular factors such as the copper ligation pattern, the polarity of the protein environment and the solvent accessibility of the metal site responsible for its modulation is of utmost importance. Several studies have demonstrated that a weak axial bond at the T1 copper site preferentially destabilizes the oxidized state, and is therefore, a key factor for the high reduction potentials (400–700 mV) of blue copper sites in MCOs [1]. Previously we have shown that the replacement of Met^{502} (weakly co-ordinating to the T1 copper) in CotA laccase by the non-co-ordinating residues leucine and phenylalanine allowed the maintenance of the T1 copper geometry while causing an increase in the redox potential by 100 mV [6]. Nevertheless, mutations of the axial ligand have a profound impact on the thermodynamic stability of the enzyme and no direct correlation was found between the redox potentials

Abbreviations used: ABTS, 2,2′-azinobis-(3-ethylbenzothiazoline-6-sulfonic acid; CE, continuum electrostatic; CT, charge transfer; 2,6-DMP, 2,6-dimethoxyphenol; MC, Monte-Carlo; MCO, multi-copper oxidase; PEG, poly(ethylene) glycol; RR, resonance Raman; SGZ, syringaldazine.

[1] To whom correspondence should be addressed (email lmartins@itqb.unl.pt).

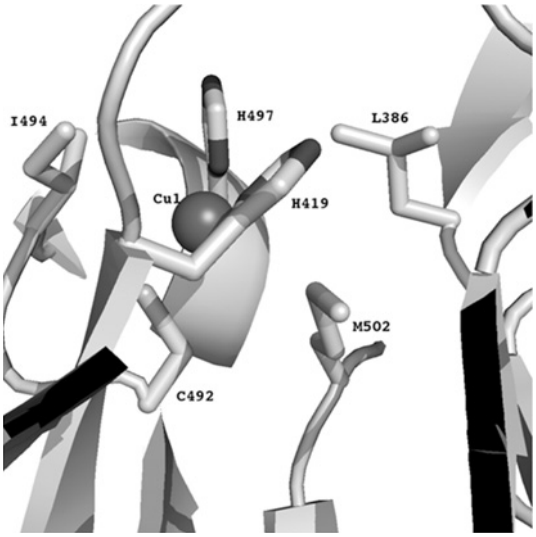

Figure 1 Structural detail of the T1 copper site in the native CotA laccase structure showing the hydrophobic Ile[494] and Leu[386] residues [7]

and the oxidation rates of the enzyme, as lower turnover rates were measured for both mutants. In the present study site-directed mutagenesis has been used to replace the residues Ile[494] and Leu[386] in the CotA laccase by an alanine residue in order to change the hydrophobic environment of the T1 copper site, namely the hydrophobic patch surrounding its His[497] ligand (Figure 1). This latter residue is exposed to the solvent and is presumably involved in the electron transfer pathway from reduced substrates to T1 copper [8]. The effect of the replacements of hydrophobic Ile[494] and Leu[386] on the T1 copper of CotA laccase have been examined by various spectroscopic techniques (UV–visible, EPR and RR) and by X-ray crystallography. In the case of the L386A mutant, two crystal structures have been evaluated, one for a 'fully loaded' copper sample at the medium resolution of 2.9 Å and the second for a sample significantly depleted in T2 and T3 copper ions, but at an improved resolution of 2.4 Å. The results obtained from all of these different techniques allowed for elucidation of the impact of the mutations on the redox and kinetic properties of the enzyme.

MATERIAL AND METHODS

Construction of CotA mutants

Single amino acid substitutions in the T1 copper centre were created using the QuikChange® site-directed mutagenesis kit (Stratagene). Plasmid pLOM10 (containing the wild-type CotA sequence) was used as a template [9]. The primers 5′-CGTATGGCATTGCCATGCTCTAGAGCATGAAGAC-3′ (forward) and 5′-GTCTTCATGCTCTAGAAGCATGGCAATGCCATACG-3′ (reverse) were used to generate the I494A mutant whereas the primers, 5′-CGGCAGACCCGTCGCTCTGCTTAATAACAAACGC-3′ (forward) and 5′-GCGTTTGTTATTAAGCAGAGCGACGGGTCTGC-3′ (reverse) were used to generate the L386A mutation. The presence of the desired mutations in the resulting plasmids, pLOM27 (carrying the I494A point mutation) and pLOM15 (bearing the L386A point mutation) and the absence of unwanted mutations in other regions of the insert were confirmed by DNA sequence analysis. Plasmids pLOM27 and pLOM15 were transformed into *Escherichia coli* Tuner (DE3) strains (Novagen) to obtain strains AH3547 and AH3560 respectively.

Overproduction and purification

Strains AH3517 (containing pLOM10), AH3547 and AH3560 were grown in Luria–Bertani medium supplemented with ampicillin (100 μg/ml) at 30 °C. Growth was followed until the mid-log phase ($D_{600} = 0.6$), at which time 0.1 mM IPTG (isopropyl β-D-thiogalactoside) and 0.25 mM $CuCl_2$ were added to the culture medium. The temperature was changed to 25 °C and agitation was maintained for 4 h. The agitation was then interrupted and the cells were maintained overnight at the same temperature. Such a protocol leads to a maximum occupancy of the copper sites [10]. Mutants prepared by this protocol will be referred to as 'fully loaded'. In a previous protocol involving overnight shaking [9] significant copper depletion was observed in both the T2 and T3 sites and the sample of L386A mutant prepared in this manner will be referred as 'copper depleted'. Cell harvesting and disruption and protein purification using a two-step protocol procedure were undertaken as previously described [7,9]. Purified enzymes were stored at − 20 °C until use.

UV–visible, EPR and RR spectra

UV–visible spectra were acquired using a Nicolet Evolution 300 spectrophotometer from Thermo Industries. EPR spectra were measured with a Bruker EMX spectrometer equipped with an Oxford Instruments ESR-900 continuous-flow helium cryostat. The spectra obtained under non-saturating conditions (160 μM protein content) were theoretically simulated using the Aasa and Väangard approach [11]. RR spectra were measured from the frozen sample (− 190 °C) using a confocal spectrograph (Jobin Yvon, XY) equipped with grating of 1800 lines/mm and a liquid-nitrogen-cooled back-illuminated CCD (charge-coupled-device) camera. For excitation, the 567.9-nm line of a Kr^+ laser (Coherent, Innova 300K), laser power of 5 mW at the sample, was used. Typical accumulation times were 40 s. Approx. 2 μl of 1 mM 'as purified' oxidized CotA, I494A and L386A mutants (in 20 mM Tris buffer, pH 7.6) were introduced into a liquid-nitrogen-cooled cold finger (Linkam THMS600) mounted on a microscope stage. The RR spectra (350–450 cm^{-1} region) were submitted to band-fitting analysis using Lorentzian bandshapes. The fitted band intensities and frequencies were used for determination of the intensity weighted frequency $<\nu_{Cu-S}>$ [5].

Redox titrations and enzyme assays

Redox titrations were performed at 25 °C and pH 7.6, under an argon atmosphere, and monitored by UV–visible spectroscopy (300–900 nm), using a Shimadzu Multispec-1501 spectrophotometer as described by Durão et al. [6]. The laccase-catalysed oxidation reactions of ABTS [2,2′-azinobis-(3-ethylbenzothiazoline-6-sulfonic acid)], 2,6-DMP (2,6-dimethoxyphenol) and SGZ (syringaldazine) were photometrically monitored, as previously described [6]. Kinetic data were determined from Lineweaver–Burk plots assuming that simple Michaelis–Menten kinetics was followed. The reaction mixtures contained ABTS (10–240 μM, pH 4), 2,6-DMP (10–1000 μM at pH 7 for wild-type and the L386A mutant or 100–7500 μM at pH 9 for the I494A mutant) or SGZ (1–100 μM at pH 7 for wild-type and the L386A mutant or at pH 8 for the I494A mutant). All enzymatic assays were performed at least three times.

Crystallization

Crystals of the I494A mutant were obtained at room temperature (?? °C) from a crystallization solution containing 0.1 M sodium citrate, 10 % PEG [poly(ethylene glycol) MME 5K and 14 % propan-2-ol at pH 5.5. Pale blue hexagonal prisms appeared from Q1

Table 1 X-ray data collection

Values in parentheses refer to the highest resolution shells as follows: for I494A, 1.69–1.60 Å; for L386A (fully copper loaded), 3.06–2.90 Å; and for L386A (copper depleted), 2.53–2.40 Å. ESRF, European Synchrotron Radiation Facility, Grenoble, France; SLS, Swiss Light Source, Paul Scherrer Institut, Villigen, Switzerland.

	I494A	L386A-fully copper loaded	L386A-copper depleted
Synchrotron beam line	ESRF ID14-3	ESRF ID14-2	SLS X06FA
Wavelength (Å)	0.931	0.933	0.9184
Detector Distance (mm)	150.4	275.5	250
Resolution (Å)	1.6	2.9	2.4
Space group	P3121	P3121	P3121
Cell parameters (Å)			
a	101.87	101.78	101.96
c	137.04	137.12	136.14
Mosaicity (°)	0.44	0.55	0.53
Oscillation range (°)	0.3	0.8	1.0
Oscillation angle (°)	90	96	90
No. of unique *hkl*	107969 (15440)	107199 (15756)	180374 (26244)
Completeness (%)	99.4 (98.4)	100.0 (100.0)	100.0 (100.0)
$I/\sigma(I)$	6.9 (2.1)	6.2 (2.3)	5.5 (5.6)
R_{symm}	0.064 (0.346)	0.100 (0.315)	0.076 (0.32)
Multiplicity	5.2 (3.9)	5.7 (5.8)	5.5 (5.6)

a drop containing 10.8 mg/ml of protein. In a similar manner, crystals of the L386A mutants appeared at room temperature from a crystallization solution containing 20 % PEG MME 5K, 0.1 M sodium citrate and 8 % propan-2-ol at pH 5.5 and a protein concentration of 7.9 mg/ml. Cryo conditions were provided by adding 22 % ethylene glycol to the crystallization solution or, in the case of the copper-depleted L386A crystals, 25 % glycerol was added.

X-ray data collection and refinement

Data collection was performed at 100 K using synchrotron radiation at the European Synchrotron Radiation Facility, Grenoble, France and the Swiss Light Source at the Paul Scherrer Institut, Villigen, Switzerland. Data collection details are shown in Table 1. Data sets for the I494A and L386A mutant enzymes were processed with MOSFLM [12] and scaled with SCALA [13] from the CCP4 program suite [14]. The data set for the copper-depleted L386A mutant extended to a significantly higher resolution, 2.4 Å compared with 2.9 Å for the fully loaded mutant, and hence was included in the present study. The structures were elucidated by molecular replacement using MOLREP [15]. The starting model was the CotA native structure (PDB code: 1W6L [7]) from which all the copper ions and solvent atoms had been removed. In each case only one solution was evident. Subsequent electron density syntheses enabled the location of the four copper ions in the molecule. Refinement was performed using the maximum likelihood functions implemented in REFMAC5 [16]. Rounds of conjugate-gradient sparse-matrix refinement with bulk-solvent modelling according to the Babinet principle [17] were alternated with model building using the Coot program suite [18] in combination with SigmaA weighted $2F_o-F_c$ and F_o-F_c maps [19]. After the first rounds of refinement, solvent molecules were added to the models based on standard geometrical and chemical restraints; molecules of ethylene diol, used as a cryo-protectant, were also located. In all cases, in a similar manner to the wild-type structure, the loop region between residues 89 and 97 was very poorly defined. The occupancies of the copper ions were adjusted such that their isotropic thermal vibration parameters refined approximately to the values of their local environment. For the T2 copper centre in particular, including the fully loaded mutants, assignment of full occupancy led to thermal vibration coefficients significantly higher than the local average and significant features in difference Fourier syntheses. Careful use of omit and standard difference Fourier syntheses, as well as monitoring of thermal vibration coefficients during refinement and modelling studies, enabled the identification of diatomic species in between the T3 copper sites in all cases and this was interpreted as a dioxygen-type species: refinement proceeded constraining the O–O distances to a target value of 1.08 Å. Moreover, in both fully loaded mutants, additional electron density was observed in the vicinity of Cys^{35} and this was modelled as an oxidized cysteine species occupying two distinct configurations. Details of the overall refinement and final quality of the models are shown in Table 1 in the Supplementary material at http://www.BiochemJ.org/bj/412/bj412ppppadd.htm.

Simulation studies

Simulated redox titrations [20,21] were performed for studying the equilibrium binding of protons and electrons. The methodology is based on CE (continuum electrostatic) methods and MC (Monte-Carlo) sampling of binding states. The CE calculations were performed using the package MEAD (version 2.2.0) [22,23]. The sets of atomic radii and partial charges were taken from GROMOS96 [24,25], except in the case of the metal centres, where quantum chemical calculations (see below) were used to derive charges. Dielectric constants of 80 and 10 were used for the solvent and protein respectively, which are values within the range where pK_a prediction is optimized [26]. The solvent probe radius was 1.4 Å, the ion-exclusion layer was 2.0 Å, the ionic strength was 0.1 M and the temperature was 27 °C. The program PETIT [20,21] was used for the MC sampling of proton and electron binding states. Site pairs were selected for double moves when at least one pairwise term was greater than 2 p*K* units. Averages were computed using 10^5 MC steps. In all simulations, the trinuclear centre was considered to be in the fully oxidized state, whereas the T1 copper centre was considered as titrable. Redox titrations are usually relative due to the unavailability of an E_{mod}, i.e. the redox potential of an adequate model compound in water; this is the case for the T1 copper centre. Owing to this, the experimental value for the wild-type enzyme was used to fit the redox titrations by adding a constant value to the potential so that the calculated and measured redox potentials for the wild-type enzyme were the same. The values for the mutants were then obtained relative to this. Partial charges for the two metal clusters (T1 copper and the T2 and T3 copper ions) were calculated considering model compounds with the conformation of the oxidized structure obtained previously [7]. The ligands of the metals were considered up to the C-β carbon (C-α in the case of the cysteine residue of the T1 copper). A dioxygen molecule bound to the T3 copper ions was considered, as well as the water molecule bound to the T2 copper. Single point calculations were performed using Gaussian 98 [27], with the B3LYP and the 6-31G(d) basis set for all atoms, with the exception of copper atoms, for which the 6-31G(2df) basis set was used. These calculations were employed to derive electrostatic potentials, which were then fitted using RESP [28] to calculate the partial charges. For the T1 copper, partial charges were calculated for the oxidized and reduced states, since both were required to simulate the redox titration of this group.

Other methods

Protein copper content was determined through the trichloroacetic acid/bicinchoninic acid method of Brenner and Harris [29]. The

Table 2 Copper content and spectral properties for the wild-type CotA and the I494A and L386A mutants

Units are: λ, nm; ε, $mM^{-1} \cdot cm^{-1}$

	Copper content (mol of Cu/mol of protein)	T1 λ (ε)	T3 λ (ε)
CotA wild-type	3.7 ± 0.1	609 (4.0)	330 (4.0)
L386A	4.0 ± 0.2	609 (3.3)	330 (3.0)
I494A	4.0 ± 0.2	624 (5.6)	330 (1.5)

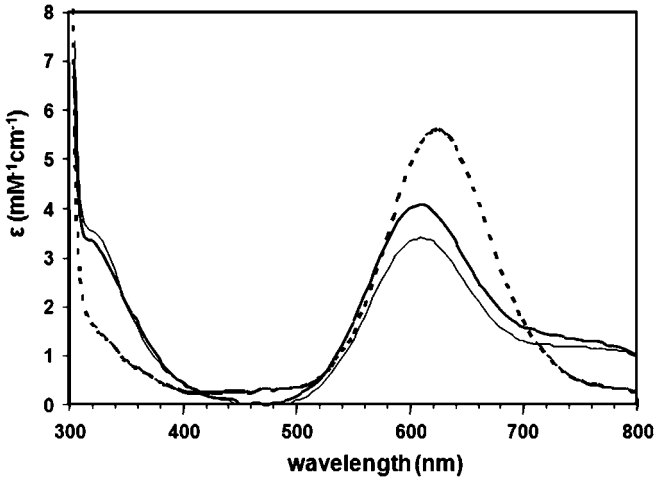

Figure 2 UV–visible spectra of wild-type CotA (solid thin line), the L386A mutant (solid thick line) and the I494A mutant (broken line)

protein concentration was measured using the absorption band of CotA laccase at 280 nm ($\varepsilon_{280} = 84739\ M^{-1} \cdot cm^{-1}$) or the Bradford assay [30] using BSA as a standard.

RESULTS AND DISCUSSION

Spectroscopic analysis of mutant enzymes

Site-directed mutagenesis replacing residues Ile^{494} and Leu^{386} with an alanine residue in the CotA laccase was undertaken in order to change the hydrophobic environment of the T1 copper centre (Figure 1). The resulting mutant enzymes showed the same chromatographic pattern during purification as the wild-type CotA laccase. Protein samples were judged to be homogeneous by the observation of a single band on Coomassie-Blue-stained SDS/PAGE. Each protein 'as isolated' contained approx. 4 mol of copper per 1 mol of protein (Table 2). Figures 2, 3 and 4 show the visible, RR and EPR spectral characteristics of the wild-type enzyme and the L386A and I494A mutants. The spectroscopic analysis of the L386A mutant revealed very subtle differences when compared with the wild-type protein, indicating minimal changes in the structure of the copper centres. On the other hand, the I494A mutant showed distinct changes in the absorption spectra such as a shift of the CT transition (T1 copper site) from 609 nm to 625 nm, a more intense blue colour (ε of 5600 instead of 4000 $mM^{-1} \cdot cm^{-1}$) and a 2-fold decrease of the extinction of the 330 nm band (a transition characteristic of the T3-coupled copper ions) (Figure 2 and Table 2). The RR spectra of the wild-type CotA, and the I494A and L386A mutants, obtained with a 567.9 nm excitation at $-190\,°C$, displayed seven vibrational bands between 350 and 440 cm^{-1} (Figure 3). Overall, the spectra bear strong similarities with those of other copper proteins

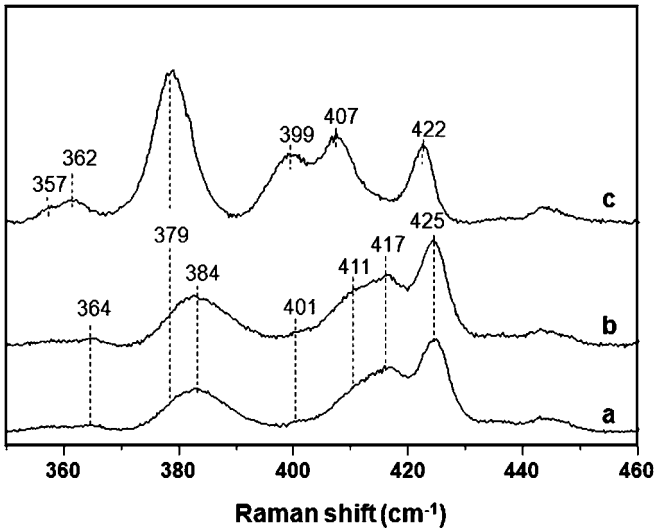

Figure 3 RR spectra of the wild-type CotA (a), the L386A mutant (b) and the I484A mutant (c), obtained with 567.9 nm excitation and 5 mW laser power at 77 K, with an accumulation time of 40s

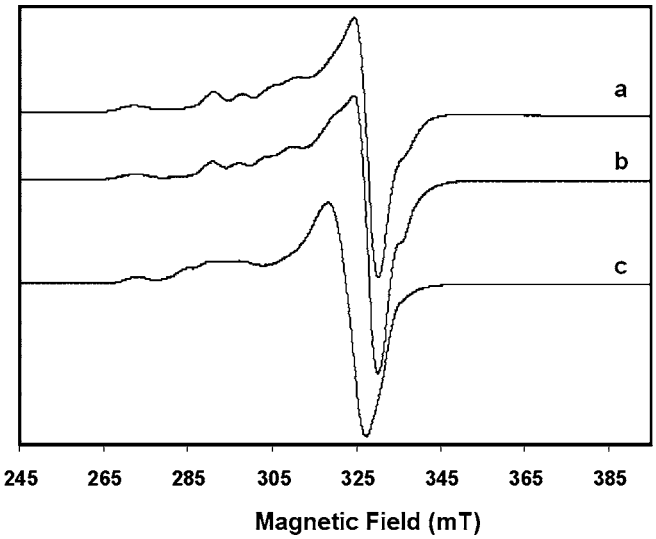

Figure 4 EPR spectra of the wild-type CotA (a), the L386A mutant (b) and the I484A mutant (c), obtained at 10 K, a microwave frequency of 9.39 GHz, 2.4 mW and a modulation amplitude of 0.9 mT

containing the T1 blue copper site [5,31–35]. However, quite different intensity distribution among the various modes in the spectrum of the I494A mutant, as compared with the wild-type protein and the L386A mutant (Figure 3), indicates a substantial perturbation of the T1 site geometry upon replacing Ile^{494} with an alanine residue. Since excitation in the resonance with the CT transition predominantly provides enhancement to the modes through the Cu–S stretching co-ordinate, its contribution to the various modes can be considered to be directly related to the relative RR intensities. Consequently, the intensity-weighted band frequencies allow determination of the intrinsic Cu–S stretching frequency, which is inversely proportional to the Cu–S bond length and thus provides a quantitative basis for description of the structural perturbation of the T1 copper site [5,31–35]. The intensity weighted band frequencies, obtained by a band-fitting analysis, include only vibrational fundamentals below 500 cm^{-1}. The value for the intrinsic Cu–S stretching frequency $<\nu_{Cu-S}>$

Table 3 EPR parameters used in the simulation of wild-type CotA, L386A and I494A mutant spectra

	Copper centres	g_{min}	g_{med}	g_{max}	A_{max} ($\times 10^{-4}$ cm^{-1})
CotA wild-type	T1	2.044	2.052	2.230	64
	T2	2.025	2.099	2.255	179
L386A	T1	2.046	2.048	2.235	64
	T2	2.025	2.095	2.258	174
I494A	T1	2.038	2.068	2.305	45
	T2	2.055	2.102	2.347	93

was found to be 410 cm^{-1} for the wild-type protein, whereas for the T1 copper site of I494A it was substantially lower (396 cm^{-1}), corresponding to a lengthening of the Cu–S(cysteine) bond for the latter. For the L386A mutant, a value very similar to the one determined for the wild-type, $<\nu_{Cu-S}> = 408$ cm^{-1}, was obtained. The EPR spectra are shown in Figure 4 and the parameters used in the simulations of these spectra are shown in Table 3. The EPR spectrum of the L386A mutant is quite similar to the wild-type, whereas the EPR spectrum and the g values, as well as the hyperfine constants of the I494A mutant reveal significant differences in both the T1 and T2 copper centres. For the T1 centre in the I494A mutant, compared with the spectrum of the wild-type, an increase in g_{max} and g_{med} values and a decrease in g_{min} value, as well as a decrease in the hyperfine constant value was observed. These observations are compatible with an increase of the distortion of the tetrahedron, which could further account for an increase in the Cu–S(cysteine) distance, as indicated by the RR results. Interestingly, both EPR and RR data indirectly suggest the existence of an altered moiety in the proximity of T1 copper of the I494A mutant. The former, based on a Vanngard–Peisach–Blumberg plot (g_{max} versus A_{max}), suggests a similarity of the T1 copper centre of the I494A mutant with the T1 copper site present in blue copper proteins having an oxygen atom as a ligand [36,37]. The latter results imply, through the weakening of the Cu–S bond, that the T1 copper ion experiences an extra electron donor interaction from the neighbouring oxygen or possibly an extra polar interaction, which may be sufficient to increase the Cu–S distance substantially [5]. The changes of the g values of T2 copper in the I494A mutant and the decrease of the A_{max} value, approaching values typical for T1 copper centres, reflect an increase in tetrahedral distortion of the T2 site. Thus the mutation of Ile^{494} in the vicinity of the T1 copper site seems to cause a perturbation in the trinuclear centre as monitored by EPR and absorption (see above). The T1 copper site is approx. 13 Å away from the trinuclear centre and is bridged through the T1 copper–Cys–His–T3 copper backbone, a possible efficient pathway for rapid intramolecular electron transfer [1–4]. Therefore taking into consideration the structural and functional closeness, it is reasonable to assume that drastic modifications of the T1 copper site in the I494A mutant, such as a lower covalency of the T1 Cu–S(cysteine) bond, could lead to alterations in the properties of the trinuclear centre.

Structural characterization of CotA mutants

The modifications of the T1 copper site geometry in the I494A and L386A mutants are clearly confirmed by the X-ray crystallography as shown in Figures 5(A) and 5(B). In the case of the L386A mutant, the T1 copper ion is barely perturbed, being co-ordinated by three strong ligands (Cys^{492}, His^{419} and His^{497}) at distances of approx. 2.1 Å, with a fourth weaker ligand, Met^{502} at a distance of 3.2 Å. However, in the case of the I494A mutant, the

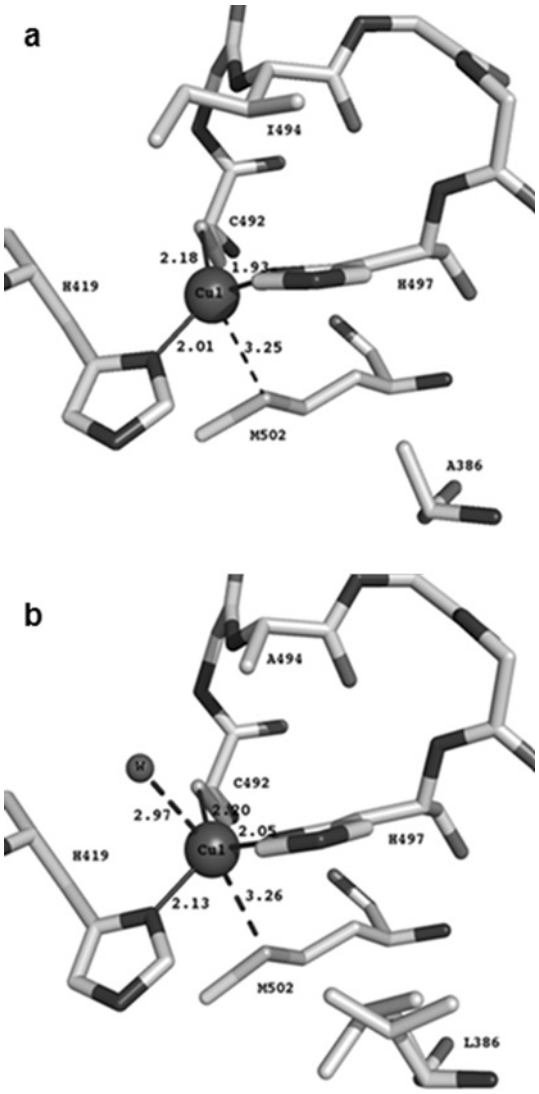

Figure 5 Structure of the T1 copper centre in the L386A mutant (a) and the I494A mutant (b)

reduction in the size of the 494 residue increases the accessibility of the T1 copper site such that a solvent molecule is able to interact with the copper ion at a distance of approx. 3.0 Å. The co-ordination geometry thus changes from distorted tetrahedral in the case of the wild-type protein and the L386A mutant, to a distorted trigonal bipyramidal in the I494A mutant. The solvent molecule itself is part of a chain of hydrogen-bonded water molecules leading to the external surface of the molecule. The resolution of the X-ray data does not, however, permit the observation of any significant change in the Cu–S bond length and therefore the strength of the bond. It therefore cannot substantiate the RR and EPR in this context. Quantitatively, the increase in accessibility [38] of the T1 copper site is approx. 418.8 Å^2. Concomitantly, the accessibility of the site to substrate molecules should also be increased, thus affecting the catalytic properties of this mutant. In addition, the X-ray structural data do not indicate any significant changes in the geometry of the T2 copper centre as indicated by the spectroscopic data. However, there has to be some flexibility at this centre in order for the water molecules, resulting from reduction of dioxygen, to access the exit solvent channel and a concomitant movement of the T2 copper may be reflected by the

Table 4 Redox potential and kinetic constants of the wild-type CotA-laccase and the L386A and I494A mutants

The redox potentials were measured at pH 7.6. The kinetic constants were measured at the optimal pH for the different substrates for each variant enzyme (see Figure 6).

		ABTS			2,6-DMP			SGZ		
	$E°$ (mV)	K_m (μM)	k_{cat} (s^{-1})	k_{cat}/K_m ($s^{-1} \cdot \mu M^{-1}$)	K_m (μM)	k_{cat} (s^{-1})	k_{cat}/K_m ($s^{-1} \cdot \mu M^{-1}$)	K_m (μM)	k_{cat} (s^{-1})	k_{cat}/K_m ($s^{-1} \cdot \mu M^{-1}$)
CotA wild-type	525 ± 10	124 ± 17	322 ± 20	2.6	227 ± 41	36 ± 5	0.16	18 ± 3	80 ± 4	4.4
L386A	466 ± 6	145 ± 3	52 ± 1	0.36	576 ± 16	17.0 ± 0.3	0.03	33 ± 1	13 ± 0.2	0.39
I494A	429 ± 27	2027 ± 193	7.2 ± 0.5	0.0036	1295 ± 73	4.5 ± 0.2	0.0035	52 ± 1	9 ± 0.1	0.17

EPR data. Furthermore, the presence of the dioxygen molecule bisecting the T3 copper ions and with the O_2 atom only some 2.5 Å distant from the T2 copper may also have some effect. Changes in its spin state in the I494A mutant may be reflected in the EPR spectra for the T2 copper ion. In the case of the L386A mutant, two crystal structures have been evaluated, one for a fully loaded copper sample at the medium resolution of 2.9 Å and the second for a sample significantly depleted in T2 and T3 copper ions, but at the improved resolution of 2.4 Å. Despite differences in copper content within the trinuclear cluster, the two L386A mutant structures are remarkably similar. There are differences in the solvent structure, but these are mainly related to the differences in the resolution of the respective data sets and consequently revealed by the respective electron density maps in details. Thus in the fully loaded L386A data set only 44 solvent molecules have been modelled. However, since the structure of the copper-depleted L386A mutant extends to a significantly higher resolution than the copper fully loaded structure and there appear to be no essential differences with respect to the copper centres, this structure can be used to provide a better definition of the T1 copper site. The geometry of the trinuclear copper centre in both the I494A and depleted L386A mutants is essentially the same as that found previously in the native structure (see for example [7]) with the optimum model incorporating a dioxygen species in between the two T3 copper atoms and almost perpendicular to their connecting vector. The presence of an oxidized cysteine residue at position 35 in the fully loaded structures is surprising and is likely to arise from the production protocol, since intense efforts have been made to minimize and to monitor radiation damage during the data collection procedures. Apart from the T1 copper centre and residue 35, the mutant enzymes show no significant structural changes with respect to the wild-type enzyme.

Redox properties of the mutants

The reduction of the T1 copper ion was measured by the disappearance of the CT absorption band in the 500–800 nm regions. The redox potentials of the T1 copper site were determined to be 525, 429 and 466 mV for the wild-type protein and the I494A and L386A mutants respectively (Table 4). These results indicate that the geometry changes at the active site have led to a stabilization of the copper(II) form of both mutants. The Cu–S(cysteine) bond strength, which can be extracted from the RR spectra, was shown to have a direct correlation with the redox potential of T1 copper sites [1,5]. The RR data qualitatively reproduce the experimental findings; an increase in the Cu–S(cysteine) bond length for the I494A mutant and a less pronounced lengthening in the case of the L386A mutant, accounting for lowering of the redox potential of both mutants, compared with wild-type.

In order to understand the physical reasons behind the changes in the redox potential, simulations of redox behaviour of the wild-type and mutant proteins were performed, using the data of the solved X-ray structures. The calculations indicate lower redox potentials for the two mutants, when compared with the wild-type, 516 mV for I494A and 510 mV for L386A. This results from a higher exposure to the solvent of the T1 copper centre in the mutants which stabilizes the oxidized state. In fact, given that the overall formal charge of the centre is +1, this is more likely to occur in a medium of higher dielectric constant such as water, than on a low dielectric constant, such as protein. The lowering of the redox potential of the mutants obtained from the calculations is not as pronounced as that observed experimentally (see above). The discrepancies may arise partially from the use of a somewhat 'unphysical' protein dielectric constant. A dielectric constant of 10 may be adequate for protonatable groups, but does not always describe the redox centres sufficiently well, specifically if they are more buried in the protein [26]. A lower protein dielectric constant results in a larger difference, but the calculation would not be as accurate for protonatable groups which may have a strong effect on nearby redox centres. For instance, calculations with an internal dielectric constant of four (results not shown), result in larger differences between the mutants and the wild-type. Moreover, the calculations show a lower decrease of the redox potential for I494A than for L386A, when compared with the wild-type, in disagreement with the experiment. For the I494A mutant, the presence of the additional water molecule at the T1 copper site cannot be properly handled by the current methodologies due to its most likely quantum mechanical nature, which goes beyond a simple solvation effect (as our calculations would model it). Nevertheless, and in a qualitative way, the water molecule, by orienting the negative oxygen atom towards the copper ion will probably stabilize the positive oxidized state, thereby decreasing the redox potential even more than shown by the calculations presented in the current study. Despite the fact that our calculations are not able to model this in full extent, they show, by comparison of the results obtained for the two mutants, that this effect is an important one, since it can change substantially what could be obtained by unspecific solvation effects.

Catalytic properties of mutant enzymes

Three substrates, one non-phenolic (ABTS) and two phenolic (2,6-DMP and SGZ) were used to determine specific changes of the catalytic properties of the mutant enzymes. Table 4 shows that the I494A and L386A mutants have higher values for the K_m and lower k_{cat} values when compared with the wild-type enzyme. The L386A mutant exhibits an approx. 2-fold increase in the K_m for all tested substrates and a 2- to 6-fold decrease of k_{cat} values. The I494A mutant is more severely compromised in its catalytic activity. Major alterations on the enzyme affinity for different substrates were observed (up to 20-fold higher K_m values as compared with wild-type) indicating that this mutation must have caused a change in the substrate-binding pocket,

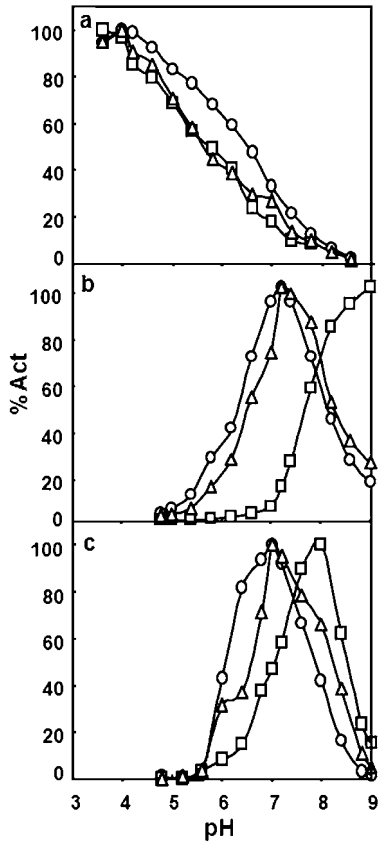

Figure 6 pH profile for catalytic activities

ABTS (**a**), 2,6-DMP (**b**) and SGZ (**c**) were used as substrates for wild-type CotA (○), the I494A mutant (□) and the L386A mutant (△).

as indicated by X-ray results. In addition, significant changes were found for the values of k_{cat}; a lowering by a factor of 10 to nearly 50 for the phenolic and non-phenolic substrates respectively. The parameter k_{cat} depends on the rate-limiting step in the turnover of multi-copper oxidases, which was shown to be the reduction of the T1 copper site [1]. According to the Marcus theory k_{ET}, a major component of the parameter k_{cat}, is dependent on three factors: the donor–acceptor electronic coupling, the reorganization energy and the redox potentials [39]. The lower redox potential determined for both mutants lead to a decreased thermodynamic driving force and thus to a decreased electron transfer rate and hence to lower k_{cat} values. In the case of the Ile^{494} mutant, major alterations of the structure near the T1 copper site were observed including a higher solvent accessibility. The reduction of this site may therefore require an increase in the reorganization energy, which in turn could result in lower k_{ET} and thus lower k_{cat} [32,33]. The mutation I494A leads to a shift in the optimal pH by approx 2 units for 2,6-DMP and 1 unit for SGZ, towards higher values, but not for ABTS (Figure 6). It has been shown that oxidation of a phenolic substrate depends on its protonation state; the deprotonated phenol has a lower redox potential and, therefore, is more easily oxidized [40]. A careful analysis of the protonation behaviour of nearby groups of the substrate binding pocket in the I494A mutant did not reveal any significant difference in their protonation behaviour compared with the wild-type enzyme. Therefore the altered pH-dependence found for phenolic substrates might be attributable to altered protonation equilibrium of the phenolic substrates themselves in the T1 substrate binding pocket of the I494A mutant, corroborating the changes at this pocket as revealed by increased K_m values. This effect would not be observed for ABTS because there is no protonation equilibrium for this substrate.

Concluding remarks

It is known that the redox potentials exhibited by the T1 copper sites of laccases span over a broad range of values, from 400 mV for plant laccases to 790 mV for some fungal laccases [1,4]. The reasons for the wide potential range among laccases are not yet fully understood. Since a high redox potential increases the range of oxidizable substrates and improves the effectiveness and versatility of the enzyme it is important to obtain a detailed description of the structure and reactivity of variants in the vicinity of the T1 copper site in order to be able to fine-tune its properties by protein engineering techniques. The redox potential of T1 copper sites can be influenced by a variety of factors, including the solvent accessibility of the metal centre and the electrostatic interactions between the metal centre and the protein [1]. Most of the site-directed mutagenesis at the T1 copper site studies has been applied to simple blue copper proteins (possessing one T1 copper site) in an effort to elucidate their electron transfer mechanism [1] and the results of a similar approach for multi-copper oxidases are yet scarce [6,32,41–44]. In the present study the crystal structures of the I494A and L386A mutants show that substitutions of hydrophobic residues with an alanine residue in the vicinity of the T1 copper site has increased the solvent accessibility, and consequently caused a decrease of the redox potential of the metal centre of both mutants. The larger cavity observed in the I494A mutant allowed for the specific binding of a water molecule to the T1 copper ion, leading to a change in the co-ordination geometry of this site, from distorted tetrahedral in the case of wild-type and the L386A mutant to a more trigonal bipyramidal in the I494A mutant. This resulted in a increased Cu–S(cysteine) bond length as observed by RR, and significant differences in the g values and the copper hyperfine coupling constant of the T1 copper in the EPR spectra. These geometrical and electronic changes further stabilized the oxidized state of the T1 copper site, resulting in a lower redox potential for the I494A enzyme as compared with the L386A mutant. As expected, the lower redox properties of the I494A and L386A mutants correlate well with their lower reactivity towards standard substrates. Therefore these results and our previous data [6] show that changes in amino acid residues in direct contact to the metal centre (including ligands) significantly affect the properties of T1 copper sites of laccases and suggest that modulation of redox potential without compromising the overall reactivity may be performed through changes in residues away from this immediate contact shell.

This work was supported by POCI/BIO/57083/2004 and FP6-NMP2-CT-2006-026456 (BIORENEW) project grants. The provision of synchrotron radiation facilities and the assistance of the staff at those facilities for help with X-ray data collection are sincerely acknowledged at the European Synchrotron Radiation Facility in Grenoble, France and the Swiss Light Source at the Paul Scherrer Institut, Villigen, Switzerland. Z. C. holds a FCT post-doctoral fellowship (SFRH/BPD/27104/2006).

REFERENCES

1 Solomon, E. I., Sundaram, U. M. and Machonkin, T. E. (1996) Multicopper oxidases and oxygenases. Chem. Rev. **96**, 2563–2605
2 Messerschmidt, A. (1997) Multicopper oxidases (A, Messerschmidt, ed.). Singapore: World Scientific
3 Lindley, P. F. (2001) Multi-copper oxidases, In Handbook on Metalloproteins. (Bertini I., Sigel, A. and Sigel, H., eds) pp. 763–811, Marcel Dekker, New York
4 Stoj, C. S. and Kosman, D. J. (2005) Copper proteins: oxidases, In Encyclopedia of Inorganic Chemistry Vol II, 2nd Ed. (King, R.B., ed). pp. 1134–1159, John Wiley & Sons

5 Blair, D. F., Campbell, G. W., Schoonover, J. R., Chan, S. I., Gray, H. B., Malmstrm, B. G., Pecht, I., Swanson, B. I., Wooddruff, W. H., Cho, W. K. et al. (1985) Resonance raman studies of blue copper proteins: effect of temperature and isotopic substitutions. Structural and thermodynamic implications. J. Am. Chem. Soc. **107**, 5755–5756

6 Durão, P., Bento, I., Fernandes, A. T., Melo, E. P., Lindley, P. F. and Martins, L. O. (2006) Perturbations of the T1 copper site in the CotA laccase from *Bacillus subtilis*: structural, biochemical, enzymatic and stability studies. J. Biol. Inorg. Chem. **11**, 514–526

7 Bento, I., Martins, L. O., Gato, G. L., Carrondo, M. A. and Lindley, P. F. (2005) Dioxygen reduction by multicopper oxidases: a structural perspective. Dalton Trans. **21**, 3507–3513

8 Enguita, F. J., Marcal, D., Martins, L. O., Grenha, R., Henriques, A. O., Lindley, P. F. and Carrondo, M. A. (2004) Substrate and doxygen binding to the endospore CotA laccase from *Bacillus subtilis*. J. Biol. Chem. **279**, 23472–23476

9 Martins, L. O., Soares, C. M., Pereira, M. M., Teixeira, M., Jones, G. H. and Henriques, A. O. (2002) Molecular and biochemical characterization of a highly stable bacterial laccase that occurs as a structural component of the *Bacillus subtilis* endospore coat. J. Biol. Chem. **277**, 18849–18859

10 Durão, P., Chen, Z., Fernandes, A. T., Hildebrandt, P., Murgida, D. H., Todorovic, S., Pereira, M. M., Melo, E. P. and Martins, L. O. (2008) Copper incorporation into recombinant CotA laccase from *Bacillus subtilis*: characterization of fully copper loaded enzymes. J. Biol. Inorg. Chem. **13**, 183–193

11 Aasa, R. and Väangard, V. T. (1975) EPR signal intensity and powder shapes: A reexamination. J. Magnet. Reson. **19**, 308–315

12 Leslie, A. G. W. (2006) The integration of molecular diffraction data. Acta Crystallogr. Sect. D Biol. Crystallogr. **62**, 48–57

13 Evans, P. (2006) Scaling and assessment of data quality. Acta Crystallogr. Sect. D Biol. Crystallogr. **62**, 72–82

14 CCP4 (1994) Collaborative computational project. Number 4. Acta Crystallogr. Sect. D Biol. Crystallogr. **50**, 760–763

15 Vagin, A. and Teplyakov, A. (1997) MOLREP: an automated program for molecular replacement. J. Appl. Crystallogr. **30**, 1022–1025

16 Murshudov, G. N., Vagin, A. A., Lebedev, A., Wilson, K. S. and Dodson, E. J. (1999) Efficient anisotropic refinement of macromolecular structures using FFT. Acta Crystallogr. Sect. D Biol. Crystallogr. **55**, 247–255

17 Tronrud, D. (1996) The limits of interpretation, CCP4 Study Weekend Macromolecular Refinement, pp 1–10

18 Emsley, P. and Cowtan, K. (2004) Coot: model-building tools for molecular graphics. Acta Crystallogr. Sect. D Biol. Crystallogr. **60**, 2126–2132

19 Read, R. J. (1986) Improved Fourier coefficients for maps using phases from partial structures with errors. Acta Crystallogr. Sect. A Found. Crystallogr. **42**, 140–149

20 Baptista, A. M., Teixeira, V. H. and Soares, C. M. (2002) Constant-pH molecular dynamics using stochastic titration. J. Chem. Phys. **17**, 4184–4200

21 Teixeira, V. H., Soares, C. M. and Baptista, A. M. (2002) Studies of the reduction and protonation behaviour of tetrahaem cytochromes using atomic detail. J. Biol. Inorg. Chem. **7**, 200–216

22 Bashford, D. and Gerwert, K. (1992) Electrostatic calculations of the p*K*a values of ionizable groups in bacteriorhodopsin. J. Mol. Biol. **224**, 473–486

23 Bashford, D. (1997) An object-oriented programming suite for electrostatic effects in biological molecules. In Scientific Computing in Object-Oriented Parallel Environments (Ishikawa, Y., Oldehoeft, R. R., Reynders, J. V. W. and Tholburn, M., eds.), pp. 233–240, Springer Berlin: ISCOPE97

24 Scott, W. R. P., Hünenberger, P. H., Tironi, I. G., Mark, A. E., Billeter, S. R., Fennen, J., Torda, A. E., Huber, T., Krüger, P. and van Gunsteren, W. F. (1999) The GROMOS biomolecular simulation program package. J. Phys. Chem. **103**, 3596–3607

25 van Gunsteren, W. F., Billeter, S. R., Eising, A. A., Hunenberger, P. H., Kruger, P., Mark, A. E., Scott, W. R. P. and Tironi, I. G. (1996) Biomolecular simulation: the GROMOS96 manual and user guide, Zurich, Groninger: BIOMOS b.v.

26 Teixeira, V. H., Cunha, C. A., Machuqueiro, M., Oliveira, A. S., Victor, B. L., Soares, C. M. and Baptista, A. M. (2005) On the use of different dielectric constants for computing individual and pairwise terms in poisson-boltzmann studies of protein ionization equilibrium. J. Phys. Chem. B Condens. Matter Mater. Surf. Interfaces Biophys. **109**, 14691–14706

27 Frisch, M. J., Trucks, G. W., Schlegel, H. B., Scuseria, G. E. Robb, M.A., Cheeseman, J.R., Zakrzewski, V.G. Montgomery, J., Stratmann, R. E., Burant, J. C. et al. (1998) Gaussian 98, Revision A.7, Pittsburgh PA: Gaussian, Inc.

28 Bayly, C. I., Cieplak, P., Cornell, W. D. and Kollman, P. A. (1993) A well-behaved electrostatic potential based method using charge restraints for deriving atomic charges: the RESP model. J. Phys. Chem. **97**, 10269–10280

29 Brenner, A. J. and Harris, E. D. (1995) A quantitative test for copper using bicinchoninic acid. Anal. Biochem. **226**, 80–84

30 Bradford, M. M. (1976) A rapid and sensitive method for the quantification of microgram quantities of protein utilizing the principle of protein-dye binding. Anal. Biochem. **72**, 248–254

31 Dave, B. C., Germanas, J. P. and Czernuszewicz, R. S. (1993) The first direct evidence for copper(II)-cysteine vibrations in blue copper proteins: resonance raman spectra of ^{34}S-Cys-labeled azurins reveal correlation of copper-sulfur stretching frequency with metal site geometry. J. Am. Chem. Soc. **115**, 12175–12176

32 Palmer, A. E., Randall, D. W., Xu, F. and Solomon, E. I. (1999) Spectroscopic studies and electronic structure description of the high potential Type 1 copper site in fungal laccase: insight into the effect of the axial ligand. J. Am. Chem. Soc. **121**, 7138–7149

33 Machonkin, T. E., Quintanar, L., Palmer, A. E., Hassett, R., Severance, S., Kosman, D. J. and Solomon, E. I. (2001) Spectroscopy and reactivity of the Type 1 copper site in Fet3p from *Saccharomyces cerevisiae*: correlation of structure with reactivity in the multicopper oxidases. J. Am. Chem. Soc. **123**, 5507–5517

34 Green, M. T. (2006) Application of badger's rule to heme and non-heme iron-oxygen bonds: an examination of ferryl protonation states. J. Am. Chem. Soc. **128**, 1902–1906

35 Qiu, D., Dong, S., Ybe, J., Hecht, M. and Spiro, T. M. (1995) Variations in the Type 1 copper protein coordination group: resonance raman spectrum of ^{34}S-, ^{65}Cu-, and ^{15}N-labeled plastocyanin. J. Am. Chem. Soc. **117**, 6443–6446

36 Andrew, C. R., Yeom, H., Valentine, J. S., Karlsson, B. G., Bonander, N., Pouderoyen, G., Canters, G. W., Loehr, T. M. and Sanders-Loehr, J. (1994)?? ??? J. Am. Chem. Soc. **116**, 11489–11498 Q2

37 Diederix, R. E. M., Canters, G. W. and Dennison, C. (2000) The Met99Gln mutant of amicyanin from *Paracoccus versutus*. Biochemistry **39**, 9551–9560

38 Binkowski, T. A., Naghibzadeh, S. and Liang, J. (2003) CASTp: computed atlas of surface topography of proteins. Nucleic Acids Res. **31**, 3352–3355

39 Moser, C. C. and Dutton, P. L. (1996) In Protein electron transfer, (Bendall, D.S., ed.), pp. 1–21 Bios Scientific Publishers Ltd

40 Xu, F. (1997) Effects of redox potential and hydroxide inhibition on the pH activity profile of fungal laccases. J. Biol. Chem. **272**, 924–928

41 Xu, F., Berka, R. M., Wahleithner, J. A., Nelson, B. A., Shuster, J. R., Brown, S. H., Palmer, A. E. and Solomon, E. I. (1998) Site-directed mutations in fungal laccase: effect on redox potential, activity and pH profile. Biochem. J. **334**, 63–70

42 Xu, F., Palmer, A. E., Yaver, D. S., Berka, R. M., Gambeta, G. A., Brown, S. H. and Solomon, E. I. (1999) Targeted mutations in a *Trametes villosa* laccase. Axial perturbation of the T1 copper. J. Biol. Chem. **274**, 12372–12375

43 Palmer, A. E., Szilagyi, R. K., Cherry, J. R., Jones, A., Xu, F. and Solomon, E. I. (2003) Spectroscopic characterization of the Leu513His variant of fungal laccase: effect of increased ligand interaction on the geometric and electronic structure of the Type 1 Cu site. Inorg. Chem. **42**, 4006–4017

44 Madzak, C., Mimmi, M. C., Caminade, E., Brault, A., Baumberger, S., Briozzo, P., Mougin, C. and Jolivalt, C. (2006) Shifting the optimal pH of activity for a laccase from the fungus *Trametes versicolor* by structure-based mutagenesis. Prot. Eng., Des. Selec. **19**, 77–84

Received 21 January 2008/25 February 2008; accepted 28 February 2008
Published as BJ Immediate Publication 28 February 2008, doi:10.1042/BJ20080166